

# Application of the SALI chaos detection method to accelerator mappings

T. Bountis<sup>a</sup> and Ch. Skokos<sup>a,b,c,1</sup>

<sup>a</sup> *Department of Mathematics, Division of Applied Analysis and Center for Research and Applications of Nonlinear Systems (CRANS), University of Patras, GR-26500 Patras, Greece*

<sup>b</sup> *Research Center for Astronomy and Applied Mathematics, Academy of Athens, Soranou Efessiou 4, GR-11527, Athens, Greece*

<sup>c</sup> *Department of Applications of Informatics and Management in Finance, Technological Institute of Mesologhi, GR-30200, Mesologhi, Greece*

**Abstract.** We apply the Smaller ALignment Index (SALI) method to a 4-dimensional mapping of accelerator dynamics in order to distinguish rapidly, reliably and accurately between ordered and chaotic motion. The main advantage of this index is that it tends *exponentially* to zero in the case of chaotic orbits, while it fluctuates around non-zero values in the case of quasiperiodic trajectories. Thus, it avoids the notorious ambiguities concerning the eventual convergence of (maximum) Lyapunov exponents to (positive) non-zero values. Exploiting the different behavior of SALI in these two cases we produce phase space ‘charts’ where regions of chaos and order are clearly identified. Evaluating the percentage of chaotic and escaping orbits as a function of the distance from the origin we are able to estimate rapidly and accurately the boundaries of the *dynamical aperture* of a proton beam, passing repeatedly through an array of magnetic focusing elements.

## INTRODUCTION

One of the basic problems in accelerator physics is the determination of the stability regions (islands of quasiperiodic motion) of a particle beam, as well as its *dynamical aperture*, i.e the domain about the ideal circular path in which the particles’ motion remains bounded [1]. In the case of ‘flat’ hadron beams, where the horizontal (x-) motion is dominant, 2-dimensional (2D) area-preserving mappings are frequently used to model the effect of nonlinearities as the particles repeatedly pass through focusing magnetic elements [2], or experience the beam-beam interaction with particles of a colliding beam [3]. The presence of invariant curves around the origin of such mappings (corresponding to the particle’s ideal circular orbit), guarantees the long-time stability of the beam. In that case, the chaotic motion that exists between these invariant curves remains always bounded and so the beam particles do not escape to infinity. On the other hand, in the case of ‘elliptical’ bunched hadron beams, where the vertical (y-) and longitudinal (z-) motion cannot be neglected and which are modelled by  $k = 2M$ -dimensional symplectic mappings with  $M > 1$ ,

chaotic regions can be connected, providing a path for the orbits to move away from the origin and eventually escape to infinity. This practically means the loss of particles in the storage rings of the accelerator and hence a reduction of the beam’s *dynamical aperture*.

In the present paper, we face the problem of the estimation of the dynamical aperture of a 4D symplectic mapping, which describes the motion of a hadron particle as it passes through a magnetic focusing element of the FODO cell type. This system has already been studied in [4, 5, 6, 7]. In particular Vrahatis et al. [7] tried to approximate invariant tori existing as far away from the origin as possible by computing stable periodic orbits of very high period. Their idea was that the corresponding islands of stability and the quasiperiodic ‘tori’ around these periodic orbits could play the role of an effective barrier of orbital diffusion, although their presence does not exclude the possible ‘leaking’ of chaotic orbits to large distances from the origin.

A more direct approach to the problem of estimating the size of the dynamical aperture, is the actual characterization of orbits on a fine grid around the origin as ordered or chaotic (escaping or not escaping to infinity). In this way one can determine the region about the ideal circular path where predominantly ordered orbits exist, thus guaranteeing the stability of the beam, at least up to the number of iterations that the orbits have been computed.

---

<sup>1</sup> E-mails: bountis@math.upatras.gr (T.B.), hskokos@cc.uoa.gr (Ch.S.)

This approach requires the use of a fast and reliable method which can distinguish between ordered and chaotic motion rapidly, reliably and accurately. The usual method of the computation of the maximal Lyapunov exponent [8, 9] does not meet these requirements as the number of iterations needed for the convergence of the Lyapunov exponent to its actual (zero or positive) value is not known a-priori and may become very high. Therefore, the application of this procedure to a huge number of initial conditions becomes impractical and its efficiency as a tool for studying the dynamical aperture of particle beams seems seriously doubtful. For these reasons, we prefer apply to our system the Smaller ALignment Index (SALI) method [10, 11, 12, 13], which has been proved to be an efficient, reliable and very fast method of chaos detection.

## THE SALI METHOD

The SALI method was introduced in [10] and has already been applied successfully to distinguish between ordered and chaotic motion in various mappings and Hamiltonian systems [11, 12, 13], as well as problems of Celestial Mechanics [14, 15], Galactic Dynamics [16, 17], Field Theory [18] as well as non-linear lattices [19, 20].

In order to recall the definition of the SALI let us consider the  $k$ -dimensional phase space of a conservative dynamical system, e. g. a  $2M$ -dimensional symplectic mapping or a Hamiltonian flow of  $N$  degrees of freedom, with  $k = 2N$ . In a symplectic mapping the evolution of an orbit with initial condition  $X(0) = (x_1(0), x_2(0), \dots, x_k(0))$ ,  $k = 2M$  is governed by the discrete-time equations of the mapping, having the form

$$X(n+1) = F(X(n)), \quad (1)$$

where  $X(n) = (x_1(n), x_2(n), \dots, x_k(n))$  is the orbit's location at the  $n$ -th iteration of the mapping. On the other hand, in a Hamiltonian flow, the motion of an orbit with initial condition  $X(0) = (x_1(0), x_2(0), \dots, x_k(0))$ ,  $k = 2N$  is governed by Hamilton's equations of motion, which have the general form

$$\frac{dX(t)}{dt} = F(X(t)), \quad (2)$$

where  $X(t) = (x_1(t), x_2(t), \dots, x_k(t))$  is the orbit's position in the phase space at time  $t$ .

Suppose we wish to determine the chaotic vs. ordered nature of an orbit  $X(n)$  of a symplectic mapping (or  $X(t)$  of a Hamiltonian system) with initial condition  $X(0)$ . To do so, one traditionally follows the evolution of one deviation vector  $V(n) = (dx_1(n), dx_2(n), \dots, dx_k(n))$  (or  $V(t)$ ), which can be considered as initially pointing to an orbit nearby the one under study, and computes the

orbit's maximal Lyapunov exponent [8, 9]. In the case of mappings the evolution of such a deviation vector  $V(n)$  is governed by the equations of motion of the so-called tangent map:

$$V(n+1) = DF(X(n)) \cdot V(n), \quad (3)$$

while, in the case of Hamiltonian flows we use the set of linear ordinary differential equations called variational equations:

$$\frac{dV(t)}{dt} = DF(X(t)) \cdot V(t), \quad (4)$$

where  $DF$  denotes the Jacobian matrix of equations (1) or (2) evaluated at the points of the orbit under study. Since, in the present paper, we study symplectic mappings, our notation from now on will be restricted to difference equations, although the following concepts can be easily extended to the case of differential equations describing Hamiltonian flows.

For the evaluation of the SALI we follow the time evolution of two initially different deviation vectors  $V_1(0)$ ,  $V_2(0)$  and define SALI [10] as:

$$\text{SALI}(n) = \min\{\|\hat{V}_1(n) + \hat{V}_2(n)\|, \|\hat{V}_1(n) - \hat{V}_2(n)\|\} \quad (5)$$

where  $\|\cdot\|$  denotes the usual Euclidean norm and  $\hat{V}_i$ ,  $i = 1, 2$  are normalized vectors with norm equal to 1, i. e.  $\hat{V}_i(n) = V_i(n)/\|V_i(n)\|$ .

Two different behaviors of SALI are thus distinguished:

1. If the orbit under study is chaotic, the two vectors  $\hat{V}_1(n)$ ,  $\hat{V}_2(n)$  tend to coincide (or become opposite) along the most unstable direction (corresponding to the maximal Lyapunov exponent). In this case, SALI tends exponentially to zero following a rate which depends on the difference between the two largest Lyapunov exponents [13].
2. If the orbit is ordered (quasiperiodic), there is no unstable direction and vectors  $\hat{V}_1(n)$ ,  $\hat{V}_2(n)$  tend to become tangent to the corresponding torus, having in general different directions. In this case SALI remains different from zero, fluctuating around some mean value [12]. An exception to this behavior appears for ordered orbits of 2D mappings where the SALI tends to zero following a power law (see [10] for more details).

The simplicity of SALI's definition, its completely different behavior for ordered and chaotic orbits and its rapid convergence to zero in the case of chaotic motion are the main advantages that make SALI an ideal chaos detection tool, perfectly suited for multidimensional conservative systems, such as proton (antiproton) beams in accelerator storage rings.

## GLOBAL DYNAMICS OF A 4D ACCELERATOR MAPPING

Consider the 4D symplectic mapping:

$$\begin{pmatrix} x_1(n+1) \\ x_2(n+1) \\ x_3(n+1) \\ x_4(n+1) \end{pmatrix} = \begin{pmatrix} \cos \omega_1 & -\sin \omega_1 & 0 & 0 \\ \sin \omega_1 & \cos \omega_1 & 0 & 0 \\ 0 & 0 & \cos \omega_2 & -\sin \omega_2 \\ 0 & 0 & \sin \omega_2 & \cos \omega_2 \end{pmatrix} \times \begin{pmatrix} x_1(n) \\ x_2(n) + x_1^2(n) - x_3^2(n) \\ x_3(n) \\ x_4(n) - 2x_1(n)x_3(n) \end{pmatrix}, \quad (6)$$

describing the instantaneous sextupole nonlinearities experienced by the dynamics of a proton beam as it passes repeatedly through magnetic focusing elements of the FODO cell type [4, 5, 6, 7]. Here  $x_1$  and  $x_3$  are the particle's horizontal and vertical deflections from the ideal circular orbit of the beam,  $x_2$  and  $x_4$  are the associated momenta and  $\omega_1$  and  $\omega_2$  are related to the accelerator's tunes  $q_x, q_y$  by

$$\omega_1 = 2\pi q_x, \omega_2 = 2\pi q_y. \quad (7)$$

Let us first examine the behavior of the SALI for some individual orbits. Vrahatis et al. [7] have computed near the boundary of escape of the mapping several stable periodic orbits of very long period, as well as some invariant tori near them. In Figure 1(a) we see the projection into the  $x_1 - x_2 - x_3$  space of one such ordered orbit of the mapping (6) for  $q_x = 0.61803$  and  $q_y = 0.4152$  first presented in figure 1(b) of [7]. This orbit is generated by a small perturbation in  $q_x$  of the stable periodic orbit of period 13237 found in [7] for  $q_x = 0.61903$  and it lies on 8 tori in the  $x_1 - x_2 - x_3$  space. The exact values of the orbit's initial condition, which will be denoted from now on as  $X^*(0) = (x_1^*(0), x_2^*(0), x_3^*(0), x_4^*(0))$ , can be found in table 3 of [7]. Following [8, 9], we may compute the maximal Lyapunov exponent  $\lambda_1$ , of the orbit as the limit for  $n \rightarrow \infty$  of the quantity

$$L_1(n) = \frac{1}{n} \ln \frac{\|V(n)\|}{\|V(0)\|}, \text{ i. e. } \lambda_1 = \lim_{n \rightarrow \infty} L_1(n), \quad (8)$$

where  $V(0), V(n)$  are deviation vectors from the orbit at  $n = 0$  and  $n > 0$  iterations respectively. We recall that  $\lambda_1 = 0$  for ordered orbits, while  $\lambda_1 > 0$  for chaotic orbits. The ordered nature of the orbit is clearly revealed by the evolution of its SALI (Figure 1(b)) and of its  $L_1$  (Figure 1(c)). The SALI remains different from zero fluctuating around  $10^{-2.5}$  converging to this value long before  $L_1$  becomes zero. Thus, as far as SALI is concerned, the computation could have been stopped after about 10000 iterations, concluding correctly that the orbit is ordered.

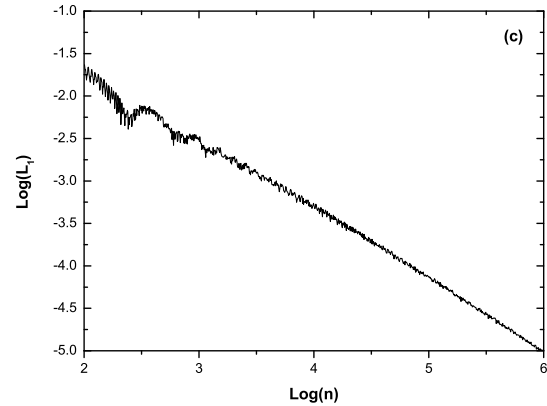
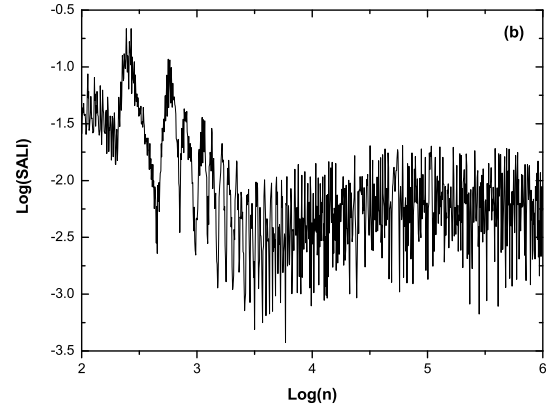
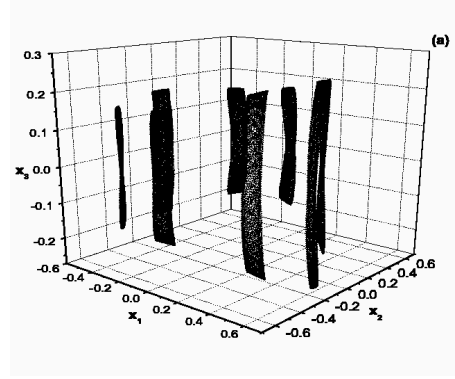


**FIGURE 1.** An ordered orbit of mapping (6). (a) Projection of 50000 consequents of the orbit into the  $x_1 - x_2 - x_3$  space. Evolution of orbit's SALI (b) and  $L_1$  (c) as a function of mapping's iterations  $n$  in log-log scale.

By changing the  $x_1$  coordinate of the initial condition of the orbit of Figure 1, to  $x_1 = 0.624$  we get the weakly chaotic orbit plotted in Figure 2(a), surrounding the 8 tori of Figure 1(a). This behavior is clearly seen in Figure

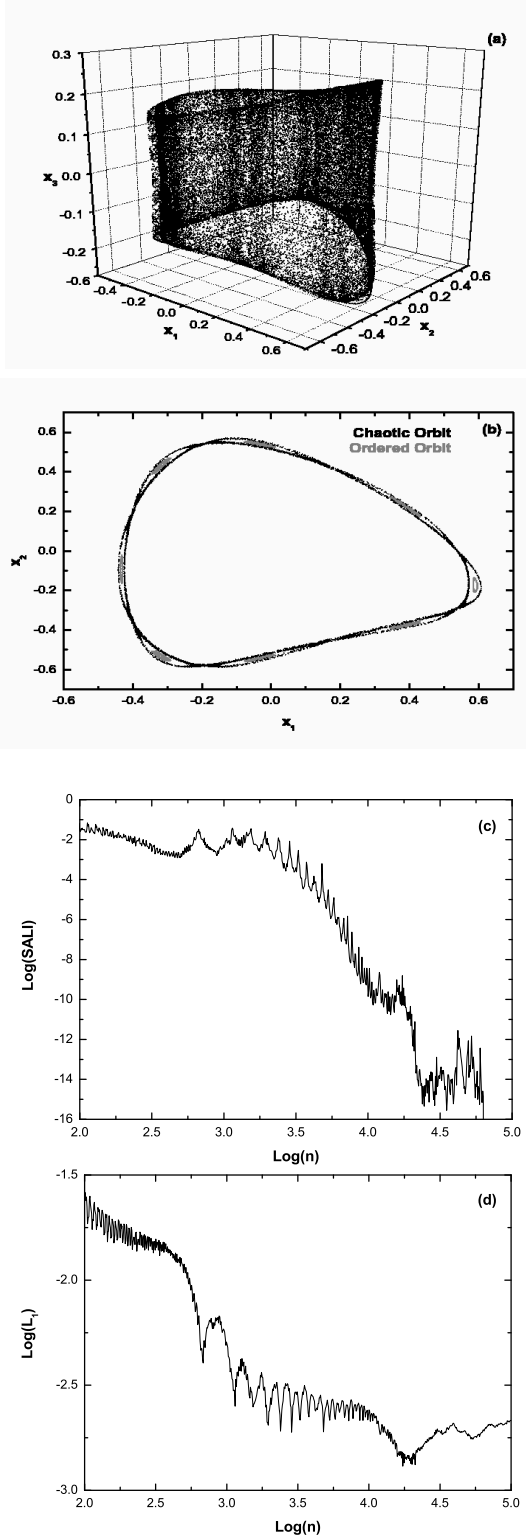


**FIGURE 2.** A chaotic orbit of mapping (6). (a) Projection of 50000 consequents of the orbit into the  $x_1 - x_2 - x_3$  space. (b) Projection on the  $x_1 - x_2$  plane of the points of panel (a) (black points) and of Figure 1(a) (gray points) with  $|x_3| \leq 0.04$ . Evolution of orbit's SALI (c) and  $L_1$  (d) as a function of mapping's iterations  $n$  in log-log scale.

2(b) where we project on the  $x_1 - x_2$  plane the points of Figures 1(a) and 2(a) with  $|x_3| \leq 0.04$ . The SALI of the chaotic orbit decreases rapidly to zero, after a transient initial phase (Figure 2(c)) reaching the limits of the computer's accuracy (i. e.  $10^{-16}$ ) after about  $n = 20000$  iterations, showing clearly the chaotic nature of the orbit. We can of course set a less demanding threshold for the SALI's values in order to define an orbit as chaotic. Considering for example as such a threshold the value  $\text{SALI} \approx 10^{-8}$ , we can characterize the orbit as chaotic after only 8000 iterations. For the same number of iterations,  $L_1$  (Figure 2(d)) does not seem to converge to a non-zero value, so that many more iterations are needed for the definite characterization of the orbit as chaotic by the use of the maximal Lyapunov exponent. In fact, at about 10000 iterations the maximal Lyapunov exponent gives an erroneous picture, as it starts to fall to values closer to zero!

In Figure 3(a) we see the projection into the  $x_1 - x_2 - x_3$  space of a chaotic orbit near the edge of the beam's dynamical aperture, with initial condition  $X^*(0)$  for  $q_x = 0.628615$ ,  $q_y = 0.4152$ , which escapes to infinity after about  $n = 82000$  iterations. Again, the SALI rapidly determines the chaotic nature of the orbit as it becomes less than  $10^{-8}$  after about  $n = 12000$  iterations (Figure 3(b)), while  $L_1$  continues to decrease showing no sign of convergence to a non-zero value, until after 32000 iterations (Figure 3(c)).

This fundamentally different behavior of the SALI for ordered (Figure 1(b)) and chaotic orbits (Figures 2(c) and 3(b)) and its rapid determination allows us to perform efficiently a more 'global' study of the dynamics of mapping (6) in order to estimate the region of stability around the origin.

As a first step in that direction, let us compute, up to  $n = 10^5$  iterations, a great number of orbits whose  $x_1(0)$  coordinate varies from 0 to 0.9 with a step equal to  $10^{-4}$ , while  $x_2(0)$ ,  $x_3(0)$ ,  $x_4(0)$  are the same as in the stable orbit of Figure 1. In Figure 4 we plot the SALI of each orbit (after  $n = 10^5$  iterations) as a function of the initial coordinate  $x_1(0)$ . We note that chaotic orbits which escape in less than  $n = 10^5$  iterations are characterized as escaping orbits and are not plotted in Figure 4. From Figure 4 we see that orbits with  $x_1(0) \leq 0.54$  are ordered, having  $\text{SALI} > 10^{-4}$ , except for a tiny interval around  $x_1(0) \approx 0.39$  where one finds chaotic orbits having  $\text{SALI} \approx 10^{-9}$ . The region  $0.54 \lesssim x_1(0) \lesssim 0.59$  is occupied mainly by chaotic orbits having SALI values less than  $10^{-8}$  and is followed by a region of mainly ordered motion for  $0.59 \lesssim x_1(0) \lesssim 0.79$ . For larger values of  $x_1(0)$  chaos dominates while escaping orbits that are not plotted in Figure 4 appear for  $x_1(0) \gtrsim 0.83$ .

Since we are interested after all in global picture of the dynamics around the origin, it is convenient to use the SALI method for 'charting' this region. Let us consider

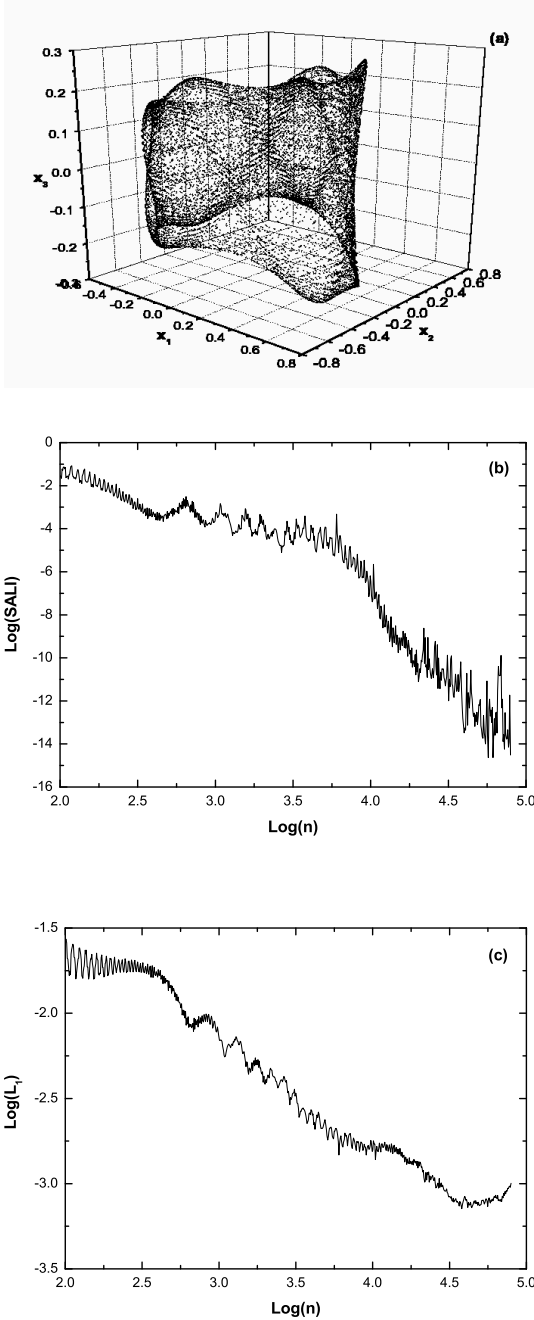


**FIGURE 3.** A chaotic escaping orbit of mapping (6). (a) Projection of 82000 consequents of the orbit into the  $x_1 - x_2 - x_3$  space. Evolution of orbit's SALI (b) and  $L_1$  (c) as a function of mapping's iterations  $n$  in log-log scale.

therefore orbits with initial conditions on a grid mesh around the origin and evolve them for a given number  $n$  of iterations. We shall characterize each orbit as chaotic if  $\text{SALI} \leq 10^{-8}$  and as ordered if  $\text{SALI} > 10^{-8}$ . If the

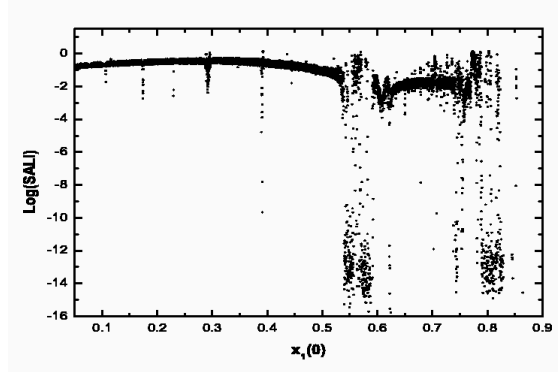


**FIGURE 4.** The values of the SALI for  $n = 10^5$  iterations of orbits with constant initial coordinates  $x_2(0), x_3(0), x_4(0)$  and  $x_1(0) \in [0, 0.9]$ , as a function of  $x_1(0)$ .

orbit escapes before the final number  $n$  of iterations is reached it will be characterized as an escaping orbit.

We first restrict our study to the 2-dimensional configuration plane  $x_1 - x_3$  in order to be able to visualize our results. In particular, we consider orbits on a  $400 \times 400$  grid mesh uniformly covering the rectangular region  $-1 \leq x_1(0) \leq 1, -1 \leq x_3(0) \leq 1$ , keeping fixed the  $x_2(0), x_4(0)$  values. The corresponding 'charts' are plotted in Figure 5 for  $x_2(0) = x_4(0) = 0$  (Figures 5(a),(b)) and for  $x_2(0) = x_4(0) = 0.1$  (Figures 5(c),(d)). The orbits were followed for  $n = 10^4$  (Figures 5(a),(c)) and  $n = 10^5$  (Figures 5(b),(d)) iterations in order to understand the evolution of 'charts' with respect to the number of iterations. In Figure 5 the initial conditions corresponding to chaotic orbits are plotted in black while the ones corresponding to ordered orbits are plotted in gray. In all panels of Figure 5 all non-colored points correspond to escaping orbits.

From the comparison of panels (a) and (b), and panels (c) and (d) of Figure 5 we see that the region occupied by non-escaping orbits (ordered and chaotic ones) does not practically change as the number  $n$  of iterations increases. This means that most of the escaping orbits fly away from the central region very fast, after a small number of iterations. So, the initial conditions plotted by black and gray color in Figure 5 define the region of stability around the beam's circular motion in the sense that all these orbits do not escape. We also see that in all panels of Figure 5 the region around the origin corresponds to ordered motion, while chaotic orbits exist mainly at the borders of the stability region. As the number of iterations increases, the number of chaotic orbits also increases. This happens because weakly chaotic orbits located at the borders of the region of ordered motion reveal their chaoticity later on as their SALI needs more iterations in order to become less than  $10^{-8}$ . Thus, although the number of non-escaping orbits remain practi-

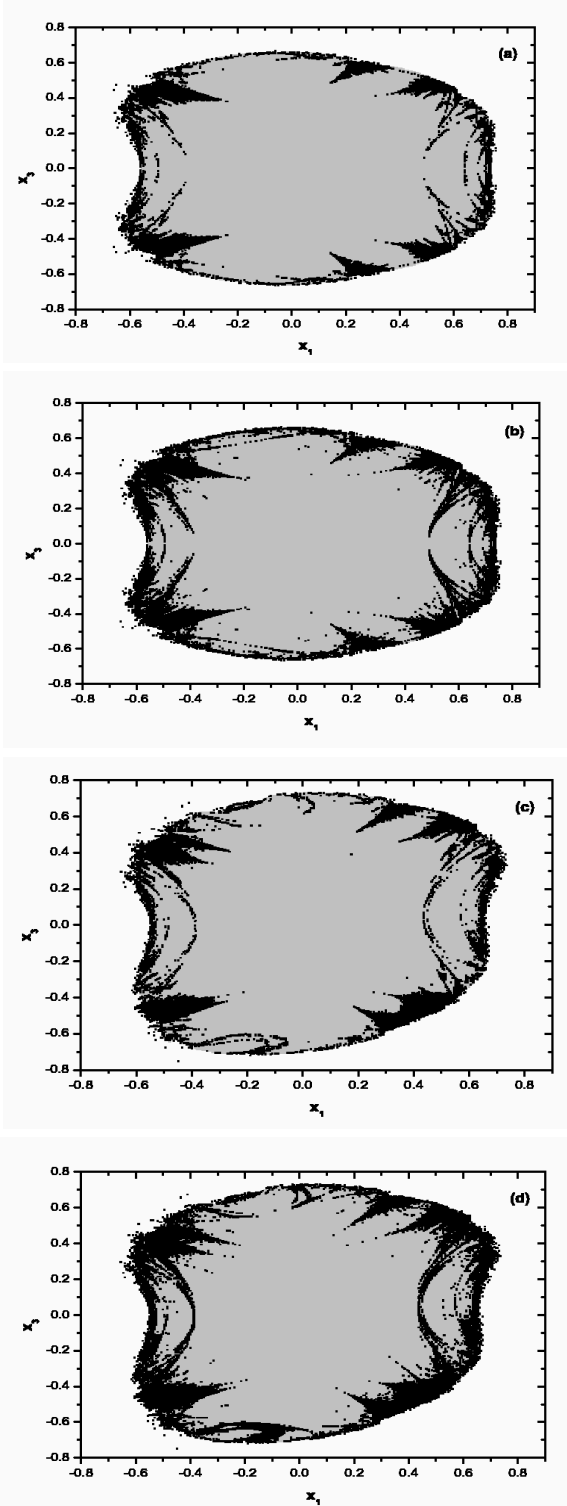


**FIGURE 5.** Regions of different values of the SALI on the  $x_1 - x_3$  plane after  $n = 10^4$  iterations (panels (a) and (c)) and after  $n = 10^5$  iterations (panels (b) and (d)). The initial conditions of the computed orbits on the  $x_2 - x_4$  plane are  $x_2(0) = x_4(0) = 0$  for panels (a) and (b) and  $x_2(0) = x_4(0) = 0.1$  for panels (c) and (d). In all frames, initial conditions are colored black if their  $\text{SALI} \leq 10^{-8}$  and gray if  $\text{SALI} > 10^{-8}$ . The uncolored initial conditions correspond to orbits that escape in less than  $n$  iterations.

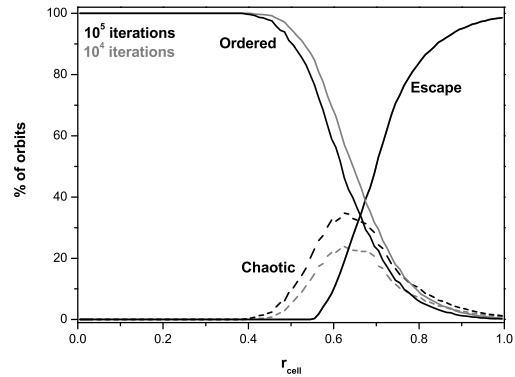


**FIGURE 6.** Percentages of ordered, escaping (solid curves) and chaotic (dashed curves) orbits, within spherical shells of width  $dr = 0.01$  as a function of shell's mean radius,  $r_{cell}$ , from the origin. The characterization of the orbits as chaotic or ordered was done according to their SALI values after  $n = 10^4$  (gray curves) and  $n = 10^5$  (black curves) iterations. The percentages of escaping orbits do not change significantly as the number of iterations increases and so the corresponding curves practically coincide.

cally constant the percentage of this number that corresponds to chaotic orbits increases as  $n$  grows.

Considering orbits with initial conditions uniformly distributed around the origin within a ‘volume’ of the full 4–dimensional phase space, we now perform a more global analysis of orbital stability. As we cannot produce plots like the ones of Figure 5 for the 4–dimensional space, we present in Figure 6 the percentages of the various types of orbits within spherical shells of width  $dr = 0.01$  inside a 4–dimensional hypersphere of radius  $r = 1$  centered at the origin. We note that by the distance  $r$  of an initial condition  $(x_1(0), x_2(0), x_3(0), x_4(0))$  from the origin  $(0, 0, 0, 0)$  we refer to the quantity

$$r = \sqrt{x_1^2(0) + x_2^2(0) + x_3^2(0) + x_4^2(0)}. \quad (9)$$

From the results of Figure 6 we see again that the number of escaping orbits does not change significantly as the number  $n$  of iterations increases, while the percentage of chaotic orbits increases with  $n$ . An estimation of the radius of the dynamical aperture therefore gives  $r \approx 0.55$ , as up to that distance from the origin no escaping orbits are found. Of course, for  $0.4 \leq r \leq 0.55$  there exists a significant amount of non–escaping chaotic orbits. So  $r \approx 0.4$  is a reasonable estimate of the maximal radius of a 4–dimensional hypersphere around the origin, where orbits not only do not escape to infinity but, in addition, are also ordered.

## CONCLUSIONS

In the present paper, we have applied the method of the Smaller Alignment Index (SALI) to the characterization of orbits of a 4D symplectic mapping describing the dynamics of a proton beam passing repeatedly through magnetic focusing elements of the FODO cell type. Thus, we have been able to locate efficiently islands of ordered motion, layers of weak chaos, as well as estimate accurately the beam's dynamical aperture.

The success of this approach lies in the fact that it can rapidly distinguish between ordered and chaotic motion in Hamiltonian flows and symplectic mappings of any dimensionality. Since the SALI decays exponentially to zero in the case of chaotic orbits (and oscillates quasiperiodically around non-zero values in ordered regions), it bypasses the slow and often irregular convergence properties of the computation of Lyapunov exponents and thus provides quickly a definite characterization of each orbit.

This allows one to use the SALI to characterize whole domains in phase space of different scales and sizes and 'chart' them as chaotic or regular. Carrying out such a study for the mapping of this paper, we have been able to 'trace out' the dynamical aperture of proton beams with a 2-dimensional (x and y) cross section, by locating 4-dimensional domains, where non-escaping behavior is guaranteed even after a very high number of iterations. Currently, we are extending our work to more realistic 6-dimensional mappings, where longitudinal (or synchrotron) oscillations are taken into consideration and space charge effects are included [21]. Despite the additional complications present in these models, we believe that the SALI method will again be able to yield useful results, 'charting' correctly the dynamics of phase space domains that would otherwise be very difficult to probe efficiently by more traditional techniques.

## ACKNOWLEDGMENTS

Ch. Skokos was partially supported by the Research Committee of the Academy of Athens and the EMPEIRIKEION Foundation. T. Bountis acknowledges the partial support of the European Social Fund (ESF), Operational Program for Educational and Vocational Training II (EPEAEK II) of the Greek Ministry of Education and particularly the Programs "HERAKLEITOS" and "PYTHAGORAS II".

## REFERENCES

1. Giovanozzi M, Scandale W and Todesco E 1997 *Part. Accel.* **56** 195
2. Bazzani A, Todesco E, Turchetti G and Servizi G 1994 *A normal form approach to the theory of nonlinear betatronic motion*, CERN, Yellow Reports 94-02
3. Bountis T, Budinsky N and Eminhizer C R 1984 *Nucl. Instr. Meth.* **227** 205
4. Bountis T C and Tompaids S 1991 *Future Problems in Nonlinear Particle Accelerators* eds G Turchetti and W Scandale (Singapore: World Scientific) p 112
5. Bountis T and Kollmann M 1994 *Physica D* **71** 122
6. Vrahatis M N, Bountis T and Kollmann M 1996 *Int. J. Bifur. & Chaos* **6**(8) 1425
7. Vrahatis M N, Isliker H and Bountis T 1997 *Int. J. Bifur. & Chaos* **7**(12) 2707
8. Benettin G, Galgani L, Giorgilli A and Strelcyn J-M 1980 *Meccanica* **March** 9
9. Benettin G, Galgani L, Giorgilli A and Strelcyn J-M 1980 *Meccanica* **March** 21
10. Skokos Ch 2001 *J. Phys. A* **34** 10029
11. Skokos Ch, Antonopoulos Ch, Bountis T and Vrahatis M N 2003 *Libration Point Orbits and Applications* eds G Gomez, M W Lo and J J Masdemont (Singapore: World Scientific) p 653
12. Skokos Ch, Antonopoulos Ch, Bountis T and Vrahatis M N 2003 *Prog. Theor. Phys. Supp.* **150** 439
13. Skokos Ch, Antonopoulos Ch, Bountis T and Vrahatis M N 2004 *J. Phys. A* **37** 6269
14. Széll A 2003 *PhD Thesis* Glasgow Caledonian University
15. Széll A, Érdi B, Sándor Zs and Steves B 2004 *MNRAS* **347** 380
16. Manos T, Athanassoula E 2005 Chaos and the dynamical evolution of barred galaxies *Preprint astro-ph/0510823*
17. Manos T, Athanassoula E 2005 Detecting chaotic and ordered motion in barred galaxies *Preprint astro-ph/0510824*
18. de Assis L P G, Helayel-Neto J A, Haas F and Nogueira A L M A 2005 On the integrability and chaos of an  $N = 2$  Maxwell-Chern-Simons-Higgs mechanical model *Preprint hep-th/0505159*
19. Panagopoulos P, Bountis T C and Skokos Ch 2004 *J. Vib. & Acoust.* **126** 520
20. Antonopoulos Ch, Bountis T C and Skokos Ch 2005 Chaotic dynamics of  $N$ -degree of freedom Hamiltonian systems *Preprint nlin.CD/0506043*
21. Benedetti C and Turchetti G 2005 *Physics Letters* **A340** 461